Electroluminescence and cathodoluminescence from inorganic CdSe nanocrystals embedded in thin films

H. Mattoussi,[#,a] J. Rodriguez-Viejo,[+,b] K. F. Jensen,[+] M. G. Bawendi,[•] and M. F. Rubner[#]

[#]Department of Materials Science and Engineering
[+]Department of Chemical Engineering
[•]Department of Chemistry
Massachusetts Institute of Technology, Cambridge, MA 02139

Abstract

Electroluminescence (EL) from heterostructure devices made of organic poly (phenylene vinylene), PPV, and inorganic semiconductor CdSe nanocrystals have been investigated, along with cathodoluminescence (CL) from thin films of ZnS doped with CdSe-ZnS core-shell nanocrystals. In the EL devices, the organic PPV structure, built next to the anode using the technique of molecular layer-by-layer sequential adsorption, serves as the hole transport layer. The inorganic layer, adjacent to the electrode and made of spin cast CdSe nanocrystals passivated with either organic groups or with a thin layer of ZnS, is the emitting layer. The ZnS host film in the CL devices, built using chemical vapor deposition, serves as the support medium for the dispersed nanocrystals, but also provides additional passivation to the surface of those nanocrystals. We find that the EL and CL signals almost exclusively originate from the inorganic nanocrystals in both cases, i.e., EL comes from the nanocrystal layer in the heterostructure device while CL is generated from the dispersed particles in the composite film. The external EL quantum efficiency, η_{EL}, is not enhanced by the presence of ZnS overcoating, opposed to the observed increase in the photoluminescence (PL) quantum yield. However, we find that the CL emission and its stability are substantially improved by the presence of ZnS around the emitting nanocrystal cores. These observations reflect a difference in the effects of overcoating on the various luminescence processes. On the one hand, a ZnS overlayer is associated with an additional energetic barrier that reduces the efficiency of charge injection into the nanocrystals for EL. On the other hand, PL and CL processes only benefit from the surface passivation with ZnS.

Introduction and background

Colloidal semiconductor nanocrystals, e.g., CdSe, CdS, InP, InAs, with particle sizes that can be varied between 10 Å and 60 Å in radius, have been made using solution chemistry routes. They are a new class of materials intermediate between the bulk and molecular scale.[1-6] Three

---

[a] Present address: Naval Research Laboratory, Optical Sciences Division, Washington, DC 20375; electronic address: hedimat@ccs.nrl.navy.mil

[b] Present address: Grupo de Fisica de Materiales I, Universidad Autónoma de Barcelona, 08193 Bellaterra SPAIN.

Part of the SPIE Conference on Organic Light-Emitting Materials and Devices II
San Diego, California • July 1998
SPIE Vol. 3476 • 0277-786X/98/$10.00

dimensional confinement of the exciton, an excited electron-hole (e-h) pair, in these nanoparticles results in size dependence of several of their spectroscopic properties, e.g., absorption and photoluminescence spectra.[1-10] Manipulation of the surface nature by attaching various organic capping groups on the particle surface has also been achieved, using the above solution chemistry routes.[11-13] This permits passivation of the surface electronic states, and improves the spectroscopic properties of these materials. For CdSe nanocrystals, the photoluminescence is further enhanced by growing a few atomic monolayers of ZnS or CdS (wider band gap semiconductors) on the surface of the native nanocrystals.[14-16] Photoluminescence quantum yields, ϕ_{PL}, of 50 to 80% have been reported with the overcoated nanocrystals.[14-16] Various studies that focused on the characterization, the understanding of the spectroscopic properties, and their dependence on the nanocrystal size and nature of the surface capping have been reported for these materials.[4-11] Additional studies focusing on the assignment of the excited states for an ensemble of nanocrystals (finite size distribution), the photoluminescence spectral resolution and the fluorescence intermittence of a single nanocrystal, have also been carried out.[10,17,18] Theoretical approaches to explain some of the above observations, e.g., origin and size dependence of the Stokes shift in these materials, have also been reported.[19]

Electroluminescence (EL) and cathodoluminescence (CL) of thin film display devices with CdSe nanocrystals emerge as two leading possible applications involving these materials. This interest is motivated by a few factors: the relatively straightforward method of making and processing these materials, the high PL quantum yields achieved, and the wide range of wavelengths that can be generated by simple control of the nanocrystal size.

In the present report, we compare studies of the electroluminescence (EL) and cathodoluminescence (CL) from thin film structures, where CdSe nanocrystals are the emitting centers for both processes. In particular, we address the effects of ZnS overcoating on the luminescence properties, i.e., electroluminescence, cathodoluminescence and photoluminescence. In the EL study we use heterostructure devices made of an organic hole transport layer (made of poly (phenylene vinylene), PPV) and a thin layer of CdSe nanocrystals, either organically capped or ZnS overcoated. The PPV layer is built next to the anode, using molecular layer-by-layer sequential adsorption, to move the excitonic recombination zone away from the anode (due to its low electron conductivity). This prevents quenching of the emission at the ITO anode. The inorganic layer serves as the electron transport layer (ETL), but also embeds the exciton recombination zone. The above heterostructure device is sandwiched between an ITO anode and an Al electrode. The cathodoluminescence study is carried out on composite films, made of CdSe-ZnS core-shell nanocrystals dispersed in a ZnS matrix. The composite films are grown using organometallic chemical vapor deposition (OMCVD). Photoluminescence studies of the above films are carried out for verification and control.

Materials and sample preparation

The CdSe nanocrystals are made from organometallic precursors (dimethyl cadmium, $CdMe_2$, and trioctyl phosphine selenide, TOPSe), using high temperature solution chemistry.[1] Nucleation, growth and annealing are carried out in a hot (300-340°C) coordinating solvent made of a mixture of trioctyl phosphine and trioctyl phosphine oxide (TOP/TOPO).[1] This procedure

provides nanocrystals capped with TOP/TOPO groups, with good control of the size and size distribution.[12,13] Overcoating the crystallites with ZnS is also carried out using the above solution chemistry method, but at lower temperatures, T ≅ 140-190°C, to avoid changes in the initial CdSe core.[14,15] This procedure provides core-shell nanocrystals with the outer surface capped with TOP/TOPO molecules. Because ZnS is a semiconductor with a wider band gap, it permits passivation of the surface states, and improves the spectroscopic properties of these materials. Effects of ZnS overcoating are reflected in the substantial increase of the photoluminescence intensity with respect to particles with pure organic capping, e.g., the photoluminescence yield, ϕ_{PL}, increases from ~ 10% (for TOP/TOPO capped CdSe nanocrystals) to ~ 50% upon growing a thin layer (~2-3 monolayers) of ZnS on the nanocrystal surface.[14,15] The data from CdSe-ZnS nanocrystals show a slight red shift (~ 5 nm or larger) of the band edge absorption with respect to crystallites with TOP/TOPO caps, caused by a slight broadening of the initial size distribution during overcoating and leakage of the exciton into the ZnS overlayer.[15] Such shift is even more pronounced with CdS overcoating.[16] In the present study, the nanocrystals are dispersed in toluene at high concentration and used for preparation of the EL devices.

The EL devices are made by spin casting from concentrated dispersions in toluene (O.D. ≅ 5-10 in a 1mm optical path cuvette) on top of the PPV self-assembled layer. Appropriate spinning angular frequencies, ω, are used to make the nanocrystal layer with the targeted thickness. The PPV based organic hole transport layer is itself a heterostructure of 2 bilayer systems. Both sublayers are processed from the precursor PPV, pPPV (a polycation), in solution using the technique of layer-by-layer sequential adsorption.[22] The first sub-layer is made of 20 alternating individually adsorbed layers (10 bilayers) of pPPV and sulfonated polystyrene, SPS. The next sub-layer is made of 40 alternating monolayers (20 bilayers) of pPPV and polymethacrylic acid PMA. The thin films are dried in vacuum, then heat converted at 210-240°C under dynamic vacuum for about 10-12 hours. This eliminates the thiophenium groups in the precursor, pPPV, and provides the final conjugated PPV.[22,23]

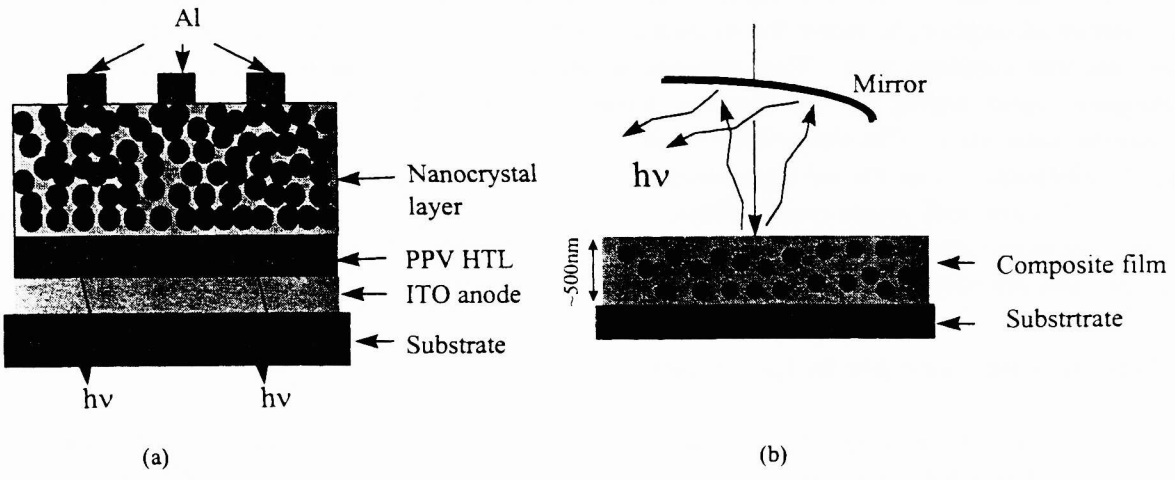

Fig.1: Sketch of the devices: **(a)** Thin film of PPV/nanocrystal heterostructure device used for EL; **(b)** Composite ZnS film doped with CdSe-ZnS core-shell nanocrystals used for CL.

The samples for CL experiments are prepared using CdSe-ZnS core-shell nanocrystals, with their initial cap exchanged from the native TOP/TOPO to pyridine, then dispersed in a mixture of anhydrous pyridine and acetonitrile (ratio 1:2). The solvent mixture has a lower surface tension, and is better suited for electrospray.[20] The incorporation of nanocrystals in ZnS thin films is carried out by electrospray organometallic chemical vapor deposition (ES-OMCVD) in a tubular flow CVD reactor equipped with an external heater.[20] The spray of nanocrystals, once fed into the reactor inlet, is mixed with a flow of hydrogen saturated with the organometallic precursors, i.e., hydrogen sulfide, H_2S, and diethyl zinc, $ZnEth_2$, (or dimethyl zinc $ZnMeth_2$). Growth temperatures range from 100 to 250°C while the pressure is maintained at ~ 600 Torr. The composite thin films, with thicknesses ranging from 500 to 1000 nm, are grown on fused silica and silicon substrates. Thin layers (~ 100 nm) of pure ZnS are grown beneath and on top of the composite film. These extra layers ensure complete coverage and protection of the nanocrystals in the composite film.

For EL, measurements of the current, I, and light power output, P, vs. applied voltage, V, are carried out simultaneously in inert atmosphere (N_2). We use a voltage source (Keithley 230), with the positive contact connected to the ITO and the negative contact connected to the Al electrode (forward bias). The current is measured on a digital multimeter (Hewlett-Packard 34401A), while the light power output is collected on a calibrated Si photodiode and measured using an optical power meter (Newport 1830C). The voltage is varied in discrete positive or negative steps, and the current and power output are measured at each step. The CL measurements have been carried out at room temperature using a scanning electron microscope (JEOL SEM) equipped with an Oxford Mono-CL spectrometer. This permits inspection of the film morphology before and after exposure to the electron beam. Typical beam currents between 1 and 200 nA and operating voltages between 1 and 40kV have been used.[20,21] The PL and EL spectra are measured in air using a Spex Fluorog-2. Absorbance measurements are carried out using a UV-Visible Near IR spectrophotometer Cary 5E.

Results and discussion

Thin film characterization and optical properties

Previous TEM cross-sectional images of nanocrystal films spun from concentrated dispersions in toluene on flat epoxy disks, and plan view images of thinner films cast on mica substrates, showed homogeneous dense nanocrystal layers, with well defined flat interfaces.[24] Furthermore, those TEM images showed that the organic capping groups (TOP/TOPO) serve to "cement" the nanocrystals together, resulting in a robust films with high mechanical integrity. This is important when considering the mechanisms for the movement of carriers in these films. The HTL thickness estimated from the TEM cross-sectional images is about 25-30 nm for the present structures.[23,24]

In Fig. 2a, we show a comparison between absorbance and photoluminescence spectra from single structures of PPV (HTL) and nanocrystals with TOP/TOPO caps (radius $R_0 \cong 23.5$ Å). The absorption spectrum of PPV thin film shows a broad peak centered around 400 nm. Fig. 2a also shows the EL spectrum from a heterostructure and the PL spectrum from a pure CdSe

nanocrystal thin film. A good superposition of the respective EL and PL peaks is observed. Moreover, the EL spectrum shows an additional small contribution at lower wavelengths, i.e., shoulder in the green region of the spectrum. That contribution results from the HTL, and has vibronic structures characteristic of PPV.[22,24] The same features are observed whether "bare" (organically capped) or Zns overcoated nanocrystals are used. The above spectra show that the nanocrystals are the primary EL emitting sources in the heterostructure. Fig. 2b shows absorption, PL and CL spectra of a composite film made of ZnS doped with CdSe-ZnS (core-shell) nanocrystals, $R_0 \cong 16.5$ Å. The absorption and PL spectra are characteristic of the dispersed nanocrystals, with a small (Stokes) shift between the first absorption peak and the PL peak (~ 15 nm). Figures 2a and 2b also show that the CL, EL, and PL spectra have similar characteristics. This indicates that the emission originates from the same state (band-edge) for all three processes, despite the fact that the creation of an e-h pair in the nanocrystal results from different sources. The excitons result from absorption of higher energy photons for PL and from transfer of a kinetic energy from incident energetic electrons (after collision) for CL, respectively. For EL, the excitons result from "injection" into the nanocrystals of electrons and holes, which migrate, in opposite directions, from the cathode and anode, respectively, upon application of a voltage. The slight red shift observed in the CL peak in comparison with that of the PL can be attributed to a quantum Stark shift. The latter is due to the presence of a strong electric field, caused by the electron flux in the sample.

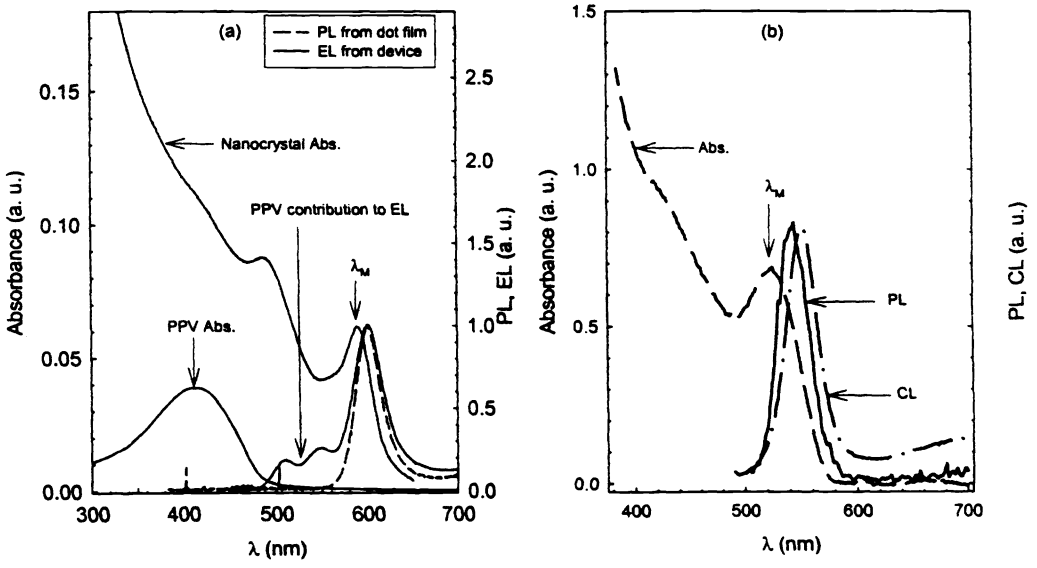

Fig. 2: (a) Absorbance spectra of single structures of PPV and nanocrystals (with $R_0 \cong 23.5$Å), along with the PL spectrum of a nanocrystal film and the EL spectrum of a heterostructure device. The PL spectrum of the nanocrystal layer and the EL spectrum of the device have the same peak location. A weak contribution to the EL spectrum from the organic HTL is observed at higher voltage. **(b)** Absorbance, PL and CL spectra of a film of ZnS doped with CdSe-ZnS nanocrystals (with $R_0 \cong 16.5$Å). A pure ZnS film is used as a reference. The CL peak has an additional red shift with respect to the PL.

In Fig. 3a, we show the normalized electroluminescence spectra for heterostructure devices using various nanocrystal sizes, where the emission peak can be tuned from yellow-green to red as the size is increased.[24,26,27] Nevertheless, we have not been able to generate stable blue-green emission from devices with smaller nanocrystals, i.e., nanocrystals with their first transition energy comparable to, or higher than that of the PPV band gap ($R_0 < 18$ Å or $Eg > 2.3$ eV and $\lambda_M < 540$ nm) do not provide measurable EL signal. Figure 3b shows the CL spectra for two films with different nanocrystal sizes, $R_0 \cong 16.5$ Å and $R_0 \cong 21$ Å. The peak position is red shifted with increasing size. With samples of CdSe-ZnS nanocrystals dispersed in ZnS films, broader spectra have been measured. In addition, more pronounced stokes shifts (mostly CL) with respect to the first absorption peak at λ_M are observed. This is caused by a larger size distribution for the core-shell particles, and a leak of the exciton into the overlayer.[15] The CL emission can be tuned from blue through green to red (490 - 650 nm) as the nanocrystal size is increased. No limitation for CL emission is found, unlike what is observed above with EL. Moreover, the CL intensity is improved with ZnS overcoating. This represents a difference between the nanocrystal electroluminescent, cathodoluminescent and photoluminescent properties (see below).

Device Performance

We verified that plots of the current vs. voltage (I-V) and the power output vs. voltage (P-V) show a rectifying device behavior, with power emission observed only in the forward bias, and a good superposition of the current and power output curves. For the samples studied, we found

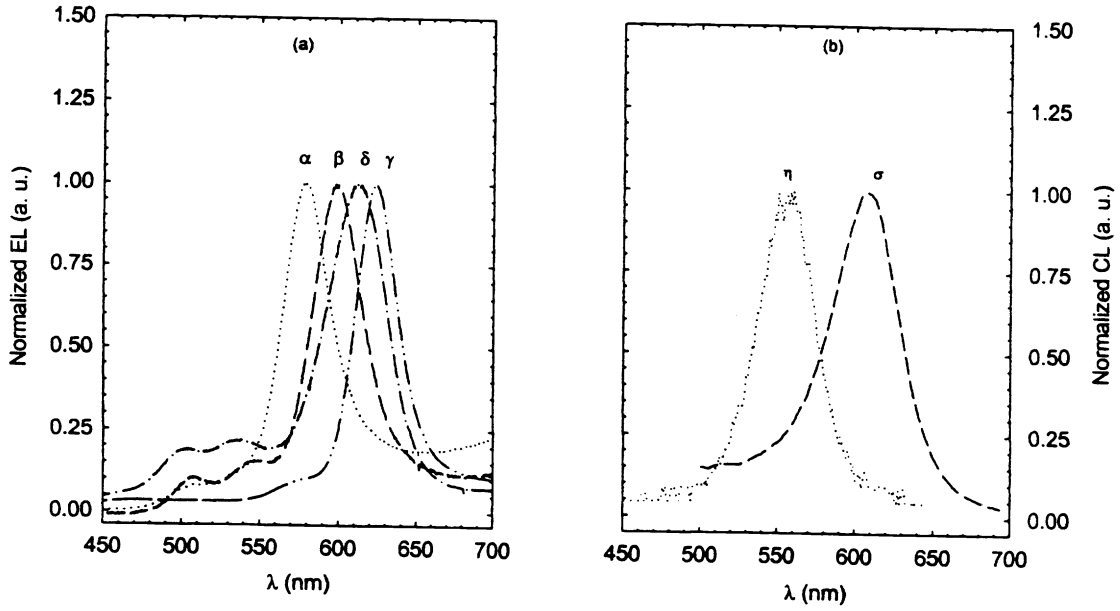

Fig. 3: (a) Continuous change of the EL emission with increasing crystallite size embedded in the heterostructure device: (α) $R_0 \cong 21$Å, (β) $R_0 \cong 23.5$Å, (δ) $R_0 \cong 25$Å, (γ) $R_0 \cong 27$Å. The EL spectra show weak contribution from the PPV in the green region of the optical spectrum. **(b)** CL spectra for two nanocrystal sizes, (η) $R_0 \cong 16.5$ Å, (σ) $R_0 \cong 21$ Å. The CL emission has always showed a larger stokes shift than the PL. Emission can be tuned by varying the nanocrystal size for both cases.

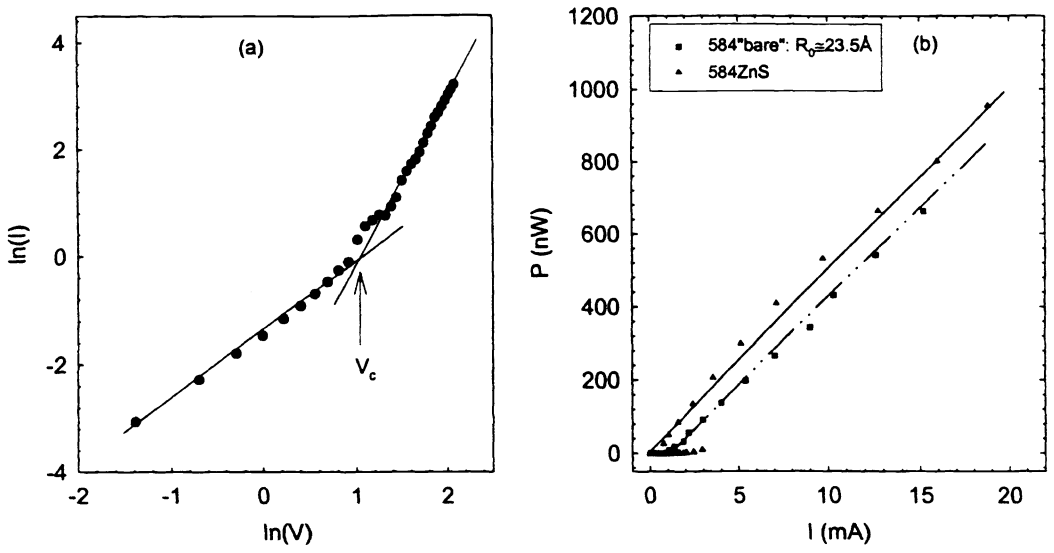

Fig. 4: **(a)** Current vs. applied voltage plotted in logarithmic scale. The turn on voltage, V_c, is defined as the intersection between the two linear regimes. **(b)** P vs. I for devices employing TOP/TOPO capped (d ≅ 100 nm) and ZnS overcoated (d ≅ 110 nm) particles. The lines are fits to the data for nonzero power output. Similar slopes imply that η_{EL} for the two devices is the same.

that the turn-on voltage, V_c, is about 3.5-4V (see Fig. 4a), independent of the film thickness (for d ≅ 20-120 nm), the nanocrystal size (for R_0 ≅ 19-27Å), and the type of capping (TOP/TOPO or low ZnS coverage). In Fig. 4, we show a comparison of P-I curves for crystallites (core size R_0 ≅ 23.5 Å) "bare" (TOP/TOPO) and ZnS overcoated (~ 1.5 monolayers). The thickness of the nanocrystal layer is about 100 nm and 110 nm for TOP/TOPO ("bare") and ZnS overcoated samples, respectively. The external quantum efficiency, η_{EL}, reaches values of about 0.1-0.2% for the present devices. The data in figure 4 also show that the EL efficiency is not greatly improved by ZnS overcoating, i.e., comparable device performance for LEDs using nanocrystals with TOP/TOPO caps or with a shallow ZnS overcoating (1-3 monolayers). Furthermore, we find that the EL emission can be strongly reduced (even eliminated) for nanocrystals with thicker ZnS overcoating (> 4 monolayers). A typical luminance power output of ~ 120-150 cd/m^2 at λ ~ 600 nm is measured (at ~ 8V) for the present heterostructure devices.

Fig. 5a shows a lifetime test for a device built with ZnS overcoated nanocrystals (23.5 Å and ~ 1.5 monolayers) at 8V. The thickness of the nanocrystal layer in the device is ~ 110 nm. The power output and the current density start with a slight increase, caused by "annealing" and releasing of traps, followed by a continuous and slow decay with time. Interruption of the voltage for about 45 min leads to a slight recovery of the power output to a level close to the initial value observed at the origin (t = 0), when the voltage is reapplied. However, the power output decreases rapidly to a level reached before interruption, then follows a slow decay with time. LEDs with lifetimes longer than 100 hrs have been made with these nanocrystals. The estimated

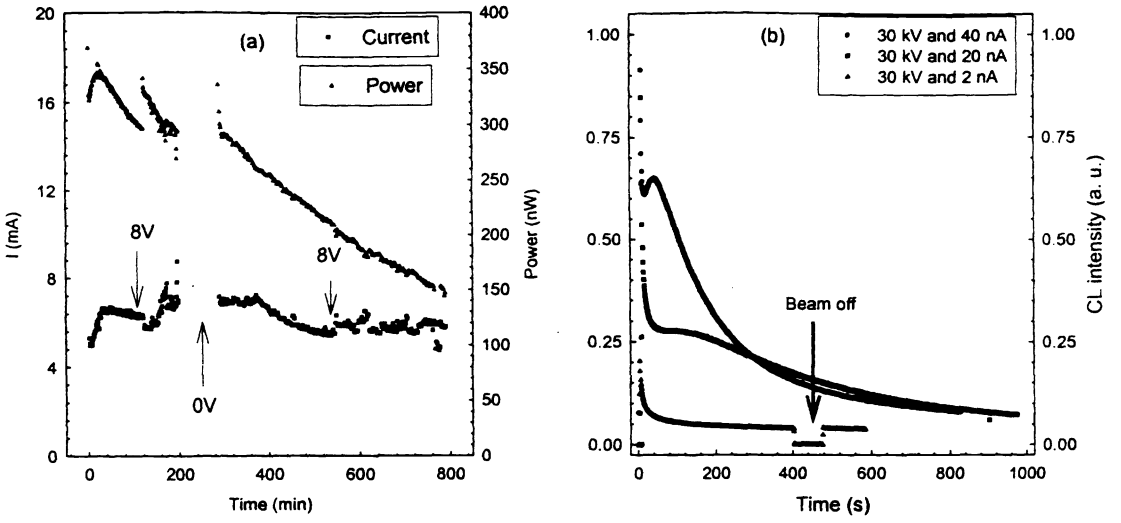

Fig. 5: **(a)** EL lifetime test for a device made using ZnS overcoated nanocrystals ($R_0 \cong 23.5$ Å). **(b)** CL lifetime tests for nanocrystal core size $R_0 \cong 21$ Å, at various incident electron energy and flux.

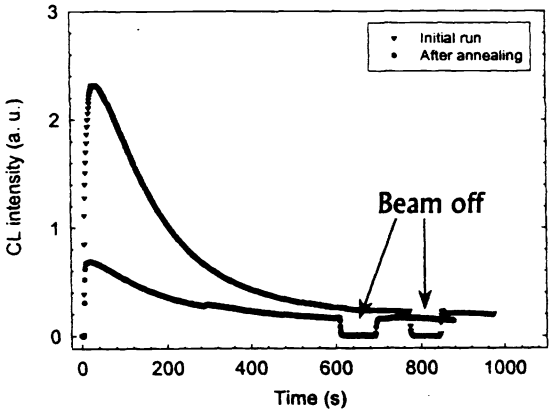

Fig. 6: CL recovery experiment using composite film ($R_0 \cong 21$ Å) before and after heating in N_2 atmosphere at 100°C for ~ 3 hrs.

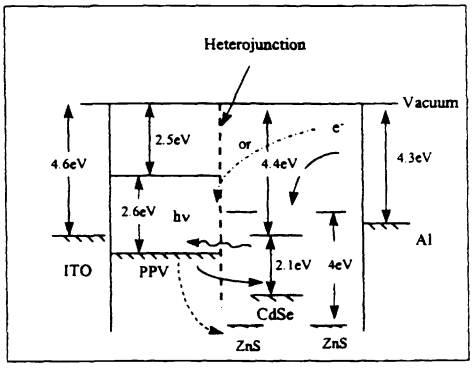

Fig. 7: Energy diagrams for devices built using "bare" and ZnS overcoated crystallites. It shows that an additional barrier is involved in the device operation with ZnS overcoating.

$t_{1/2}$ value for these devices is ~ 11 hrs from the initial stage t = 0.[24] That time is substantially larger if the initial fast decay is discarded, i.e., $t_{1/2} \cong 40$ hrs.[24]

Earlier attempts on composite films made of polymer dispersed nanocrystals (CdSe/PVK) showed that only a weak CL signal is generated. That signal decreases rapidly (~ a few seconds). Attempts using a pure film of nanocrystals (organically capped or with a ZnS shell), similar to the one used above in the EL study, also gave a weak and short lifetime signal. Nonetheless, films of pure nanocrystals but with pyridine caps, cast from solutions in pyridine, gave a slightly more stable CL signal (~1-3 min) than those in the above cases. The highest and most stable CL intensity has been generated with composite films of ZnS doped with CdSe-ZnS core-shell nanocrystals prepared by ES-OMCVD. In Fig. 5b, we show lifetime curves for a composite film doped with nanocrystals ($R_0 \cong 21$ Å) under various conditions. The CL intensity decays continuously with time. The time scales are much faster than those involved in the above EL tests, e.g., 10-20 minutes instead of hours. Fig. 5b also shows that when the electron beam is interrupted for few minutes (1-2 min), the CL intensity recovers its initial level (just before interruption), once the beam is turned on a second time. The CL intensity increases with increasing electron energy and flux, but decays faster at higher voltage, see Fig. 5b. We anticipate that the above decay of the CL signal results from a decrease in the radiative relaxation of the excitons in the nanocrystals. This can be caused by an Auger process where two excitons are created in the same nanocrystal, following a collision with an incident electron, do not relax by emitting the anticipated two photons. Instead, the first generated photon is reabsorbed by the second exciton, resulting in the expulsion of an electron into the matrix (trapped electron). The ionized nanocrystal no longer contributes to the CL signal ("dark nanocrystal"). The trapping of an electron in the matrix can also result from direct ionization of the nanocrystal following collision with an incident energetic electron. This process can also be caused by absorption of high energy photons.[28] The above traps can be deep or shallow. In an independent experiment, we attempted to activate (release) these traps by heating a film in N_2 atmosphere at ~ 100°C for 3hrs, after exposure to the electron beam for several minutes. Fig. 6 shows the lifetime tests before and after heat treatment. A clear partial recovery is observed. Higher temperatures (~ 300°C), which may activate deeper traps and would result in a better signal recovery, could not be tried because that can alter the integrity of the composite film.

Discussion

The simple method of spin casting used to form the nanocrystal emitting layer has proven to be a good approach to process these materials from solution into thin homogeneous films, densely packed, and with good mechanical integrity.[24] The data in Fig. 4 shows that embedding the nanocrystals in heterostructure devices offers the unique possibility of tuning the EL wavelength emission from yellow-green to red. It also shows that CL emission can practically be tuned over the full visible spectrum, by simply changing the nanocrystal size in the composite films. This involves a one step operation, and does not require additional chemical manipulation of the materials, as often necessitated with polymers, for example.[29,30]

The independence of the turn on voltage, V_c, from the various relevant parameters e.g., nanocrystal layer, size R_0, and nature of the surface capping, indicates that the device operation, in the present case, is governed by carrier injection mechanism, with a Schottky contact at the Al/nanocrystal interface. The PPV/ITO interface is equivalent to an ohmic contact.[31] In this mechanism, the turn on voltage depends on the barrier to injection (of electrons) into the ETL

from Al. That barrier, defined by the energy difference between the electrode and the nanocrystals, is low as shown in Fig. 7. However, the above levels for the nanocrystals are derived from the bulk values and accounting for the confinement of the electron, without taking into account the organic caps. The latter form an insulating thin layer around the inorganic core, and also between the electrode and the ETL. The change in the conduction band with the nanocrystal size is small (~ 0.2-0.3 eV whereas the average band gap is ~ 2.2 eV). This would have little effects on the Schottky barrier to injection. It would also imply that V_c has little dependence on the above parameters, e.g., size and thickness. After injection, the carriers in the inorganic layer (electrons) move by a hopping mechanism and reach the PPV/nanocrystal heterojunction. The holes tunnel into the HTL, and accumulate at the interface with the nanocrystal layer. The charge build-up on each side of the HTL/CdSe interface produces a strong electric field across the junction. The band diagram (in Fig. 7) shows that the energy levels are more favorable for flow of holes from the PPV HTL into the nanocrystal layer than for electrons into the PPV. This is due to the smaller difference between the valence bands of the two materials, i.e., $|E_v(HTL) - E_v(CdSe)| \cong 1.4$ eV whereas $|E_c(HTL) - E_c(CdSe)| \cong 1.9$ eV. A recombination zone almost exclusively "confined" to the nanocrystal layer results, as confirmed by the EL spectra shown in figures 4 and 5. At higher voltages, the electric field across the junction becomes stronger, and forces migration of a small fraction of electrons into the PPV layer, resulting in a green contribution to the EL signal.

The failure to generate blue-green emission, i.e., $\lambda_{EI} < 550$ nm, may be attributed to the wider band gap of the smaller nanocrystals. For sizes smaller than 18Å, the energy band gap becomes larger than that of the PPV. Furthermore, the size decrease affects mostly the conduction band, but not the valence band (i.e., intermediate confinement), because the effective mass of the hole is heavier than that of the electron in CdSe.[10,32] Consequently, the decrease in the nanocrystal size decreases the mismatch between the conduction bands at the PPV/CdSe interface, which could increase the rate of electron injection through the junction from the nanocrystal layer into PPV. The latter becomes comparable to the rate of hole injection from the PPV into the inorganic layer. This was confirmed by a poor device performance, with a very weak and unstable signal, with the smaller nanocrystals. Using a hole transport material that has a more favorable energy levels, i.e., wider band gap should allow one to build such organic/inorganic devices with emission in the blue-green region of the spectrum.

We conclude by discussing the effects of ZnS overcoating on the above processes, i.e., electroluminescence, cathodoluminescence and photoluminescence. For EL, the energy band diagram, drawn in Fig. 7, shows that a ZnS shell is associated with an additional energy mismatch (wider energy gap) that the carriers must overcome before reaching the CdSe core. Such a barrier reduces the flow of holes from the HTL into the nanocrystal layer, and prevents electron-hole recombination from occurring within the nanocrystal core. The recombination can be reduced to nearly zero for thicker ZnS overlayers. This additional barrier would counterbalance the improvement of radiative recombination that results from a better passivation of the surface states by ZnS compared to organic capping. Attempts to make heterostructure devices where the top inorganic layer has been made of CdSe embedded in a ZnS matrix, fabricated using the above organometallic chemical vapor deposition (OMCVD), confirmed the above observations. Only a weak green EL emission from the PPV has been detected; no contribution from the nanocrystals

in the composite film is observed. With photoluminescence and cathodoluminescence the situation is quite different. The presence of a wider band gap shell permits better passivation of the surface states, eliminating residual non-radiative recombination sites. This increases the rate of exciton radiative recombination without affecting the rate of electron-hole creation following absorption of UV photons for PL, or kinetic energy after collision with incident electrons for CL. The rate of emission from a single CdSe-ZnS nanocrystal is substantially increased in comparison with the organically capped particles.[14,15] That translates into a net improvement of the PL and CL efficiencies. Moreover, for CL, embedding the crystallites into a thin ZnS composite film also results in a device robust and resistant to incident energetic electrons. This is at the origin of the improvement of the CL signal in comparison with pure nanocrystal films. This advantage is lost with the EL when CdSe-ZnS core-shell nanocrystals are used.

Conclusion

We studied the electroluminescence of CdSe nanocrystals embedded in thin film heterostructure devices, where an organic PPV hole transport layer (HTL) is used to separate the anode from the inorganic emitting layer (ETL). In addition, investigation of cathodoluminescence and photoluminescence of composite thin films made of ZnS doped with CdSe-ZnS core-shell nanocrystals has been carried out. In both cases, we find that the emission comes exclusively from the nanocrystals. Taking advantage of quantum confinement in these nanocrystals, we have been able to continuously tune the EL emission from yellow-green to red, and the CL through the visible optical spectrum, by varying the nanocrystal size. We also find that ZnS overcoating does not produce an increase in the EL emission, unlike what is observed with photoluminescence. On the contrary, embedding the nanocrystals in a ZnS matrix substantially improves the CL intensity and its stability in comparison with pure films of nanocrystals. The difference in the effects of ZnS overcoating on the EL and CL may be attributed to the additional energy barrier to hole injection into the emitting centers for EL, associated with the ZnS overlayer (ZnS has a wider band gap). This counterbalances improvement of the radiative recombination from the cores that results from a better passivation of the nanocrystal surface. This additional energy barrier does not affect the CL and PL processes. They show only improvement upon ZnS overcoating, resulting from a better passivation of the surface states.

Acknowledgments: We thank J. Michel, B. O. Dabbousi, M. Kuno, for the stimulating discussions. JRV thanks the Direccio General de Recerca from Catalonia for a postdoctoral fellowship. MGB thanks the David and Lucille Packard Foundation, the Sloan Foundation, and the W. M. Keck Foundation for funding. This research was funded in part by NSF Grant No. DMR-91-57491 and by the NSF-MRSEC program (DMR-94-00034).

References

1. C. B. Murray, D. J. Norris, and M. G. Bawendi, *J. Am. Chem. Soc.* **115**, 8706 (1993).
2. A. A. Guzelian, J. E. B. Katari, U. Banin, A. V. Kadavanich, K. Hamad, E. Juban, A. P. Alivisatos, R. H. Wolters, C. C. Arnold, and J. R. Heath, *J. Phys. Chem.* **100**, 7212 (1996).

3. A. A. Guzelian, U. Banin, A. V. kadavanich, X. Peng, and A. P. Alivisatos, *Appl. Phys. Lett* **69**, 1432 (1996).
4. M. L. Steigerwald, A. P. Alivisatos, J. M. Gibson, T. D. Harris, R. Kortan, A. J. Muller, A. M. Thayer, T. M. Duncan, D. C. Douglas, and L. E. Brus, *J. Am. Chem. Soc.* **110**, 3046 (1988).
5. Al. Efros and A. Efros, *Fiz. Tek. Poluprovodn.* **16**, 1209 (1982). [*Sov. Phys. Semicond.* **16**, 772 (1982)].
6. A. Fojtik, H. Weller, U. Koch, and Henglein, *Ber. Bunsenges. Phys. Chem.* **88**, 977 (1984).
7. L. E. Brus, *J. Chem. Phys.* **80**, 4403 (1984).
8. L. E. Brus, *Appl. Phys.* **A53**, 465 (1991).
9. D. J. Norris, A. Sacra, C. B. Murray, and M. G. Bawendi, *Phys. Rev. Lett.* **72**, 2612 (1994).
10. D. J. Norris and M. G. Bawendi, *Phys. Rev.* **B53**, 16338 (1996), and references therein.
11. M. K. Kuno, J. K. Lee, B. O. Dabbousi, F. V. Mikulec, and M. G. Bawendi, *J. Chem. Phys.* **106**, 6869 (1997).
12. H. Mattoussi, A. W. Cumming, C. B. Murray, M. G. Bawendi, and R. Ober, *J. Chem. Phys.* **105**, 9890 (1996).
13. H. Mattoussi, A. W. Cumming, C. B. Murray, M. G. Bawendi, and R. Ober, in press *Phys. Rev.***B58**, XXXX (1998).
14. M. A. Hines and P. Guyot-Sionnest, *J. Phys. Chem.* **100**, 468 (1994).
15. B. O. Dabbousi, J. Rodrigez-Viejo, F. V. Mikulec, J. R. Heine, H. Mattoussi, R. Ober, K. J. Jensen, and M. G. Bawendi, *J. Phys. Chem.* **101**, 9463 (1997).
16. X. Peng, M. C. Schlamp, A. V. Kadavanich, U. Banin, and A. P. Alivisatos, *J. Am. Chem. Soc.*, **119**, 7019 (1997).
17. S. A. Empedocles, D. J. Norris, and M. G. Bawendi, *Phys. Rev. Lett.* **77**, 3873 (1996).
18. M. Nirmal, B. O. Dabbousi, M. G. Bawendi, J. J. Macklin, J. K. Trautman, T. D. Harris, and L. E. Brus, *Nature* **383**, 802 (1996).
19. A. L. Efros, M. Rosen, M. K. Kuno, M. N. Nirmal, D. J. Norris, and M. G. Bawendi, *Phys. Rev.* **B 54**, 4843 (1996).
20. M. Danek, K. F. Jensen, C. B. Murray, and M. G. Bawendi, *Chem. Mater.* **8**, 173 (1996).
21. J. Rodrigez-Viejo, K. J. Jensen, H. Mattoussi, J. Michel, B. O. Dabbousi, and M. G. Bawendi, *Appl. Phys. Lett.* **70**, 2132 (1997); and *MRS Proceed.* **V452**, 365 (1997).
22. A. C. Fou, O. Onitsuka, M. Ferreira, and M. F. Rubner, *J. App. Phys.* **79**, 7501 (1996).
23. O. Onitsuka, A. C. Fou, M. Ferreira, B. R. Hsieh, and M. F. Rubner, *J. App. Phys.* **80**, 4067 (1996).
24. H. Mattoussi, L. H. Radzilowski, B. O. Dabbousi, E. L. Thomas, M. G. Bawendi, and M. F. Rubner, *J. Appl. Phys.* **83**, 9675 (1998).
25. Ann Sacra, *Ph.D. Dissertation*, Massachusetts Institute of Technology (1996).
26. (a) V. L. Colvin, M. C. Schlamp, and A. P. Alivisatos, *Nature* **370**, 354 (1994).
(b) M. C. Schlamp, X. Peng, and A. P. Alivisatos, *J. Appl. Phys.* **82**, 5837 (1997).
27. B. O. Dabbousi, M. G. Bawendi, O. Onitsuka, and M. F. Rubner, *App. Phys. Lett.* **66**, 1316 (1995).
28. D. I. Chepic, Al. L. Efros, A. I. Ekimov, M. G. Ivanov, V. A. Kharchenko, I. A. Kudriatsev, and T. V. Yazeva, *J. Lumin.* **47**, 113 (1990).
29. S. Son, A. Dodabalapur, A. J. Lovinger, M. E. Galvin, *Science* **269**, 376 (1995).
30. Z. Yang, B. Hu, and F. E. Karasz, *Macromolecules* **28**, 6151 (1995), and references therein.
31. S. Karg, M. Meier, and W. Riess, *J. Appl. Phys.* **82**, 1951 (1997).
32. N. Borrelli, and D. W. Smith, *J. Non-Cryst. Solids* **180**, 25 (1994).